Using a volumetric apparatus to identify and measure the mass transfer resistance in commercial adsorbents

Using a Volumetric Apparatus to Identify and Measure the Mass Transfer Resistance in Commercial Adsorbents

Stefano Brandani[1], Federico Brandani[2], Enzo Mangano[1] and Pluton Pullumbi[2]

[1] School of Engineering, The University of Edinburgh, King's Buildings, Edinburgh, EH9 3FB, UK

[2] Centre de Recherche Paris-Saclay, Air Liquide, Paris, France

Abstract

The mass transfer coefficient is a fundamental property needed to design adsorption gas separations. A collaborative study is presented where commercial LiLSX beads used in air vacuum swing adsorption for the production of oxygen are tested in two volumetric apparatuses. The initial results based on the software available in the commercial system seemed to point to a surface barrier model for the adsorption kinetics of nitrogen, but this system is known to be macropore diffusion controlled. A detailed model of the system and a new way of representing the experimental data are used to show that the mass transfer kinetics is clearly a diffusion process. Guidelines and recommendations on which tests are needed to ensure the correct use of a volumetric system in this case are presented. Through the correct interpretation of the flow through the valve in the two volumetric apparatuses, consistency in the mass transfer time constant is achieved. The effect of using the correct diffusion time constant vs the one obtained using the traditional approach is demonstrated comparing a typical oxygen vacuum swing adsorption process. A drop in performance of nearly 15% in both productivity and energy consumption is predicted if the incorrect diffusion time constant is used.

Keywords: Macropore diffusivity; nitrogen; volumetric apparatus; adsorption; air separation.

Introduction

In 2014 the global vacuum swing adsorption (VSA) oxygen on-site market was estimated to be approximately 21,000 tpd. The main applications were: the glass industry; the steel melting industry; the mining industry where the installations are often located in remote areas difficult to be supplied by liquid oxygen; and the pulp and paper industry where oxygen is used for bleaching and water treatment. In the design of air VSA processes the fundamental properties of the adsorbents that are needed are equilibrium and kinetic parameters (Ruthven, 1984; Ruthven et al. 1994). Adsorption of nitrogen on LiLSX beads is a fast system, since the VSA process used for the production of oxygen is based on the equilibrium selectivity achieved through the small Li ions exerting a strong affinity for the quadrupole moment present in nitrogen. In this process a balance is found between the pressure drop in the column, which increases as the size of the beads is reduced, and the mass transfer resistance, which increases as the size of the beads is increased. Knowledge of the mass transfer resistance is therefore needed to determine the optimal process conditions.

Diffusion of nitrogen in LiLSX beads is macropore diffusion controlled (Ruthven et al., 1994) as one would expect given the large windows present in faujasite (Baerlocher et al., 2007), which have a dimension that is approximately twice the kinetic diameter of nitrogen. In this study we focus on the methodology to determine the diffusion time constant using commercial systems, which can be converted into the tortuosity of the beads once the equilibrium isotherm and the macropore volume and the pore size distribution are known (see for example Xu and Ruthven, 1993; and Hu et al. 2014). The tortuosity of the beads is independent of temperature and therefore temperature can be used as a variable to find the conditions for measurement of the diffusion time constant.

While the determination of mass transfer kinetics may appear to be a straightforward task, if carried out without the proper experimental checks or with inappropriate theoretical models it can lead to incorrect results (Karger and Ruthven, 1992). In addition to this, one has to consider that commercial volumetric systems are designed for the accurate measurement of equilibrium properties and care should be taken when extending their use to kinetics. Some commercial systems provide also an option for the automated regression of kinetic time constants, but this can lead to incorrect results especially for fast systems. Figure 1 shows the experimental curves obtained at the Air Liquide laboratories and analysed using the software tool available on the Belsorp

instrument. The software matches the fractional uptake for the point closest to 0.5 to the surface barrier model and the diffusion model which assume zero resistance to flow in the valve. As will be discussed in the theory section, for fast systems the calculated fractional uptake is inconsistent at short times due to the zero resistance assumption. As can be seen from the comparison of the experimental data and the models below a fractional uptake of 0.5, one could be led to conclude that the surface barrier model represents this system more accurately than the diffusion model. In this contribution this paradox is resolved and the correct diffusion time constant is derived. A short analysis of the impact of the incorrect time constant on an oxygen VSA will be presented in order to highlight the importance of measuring correctly this fundamental property.

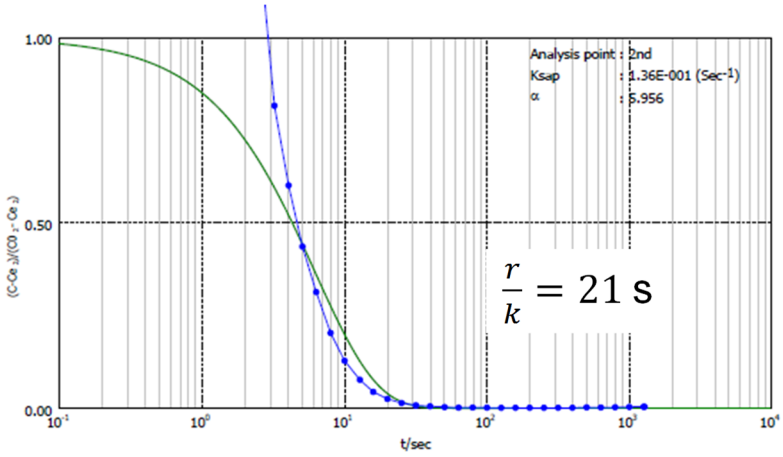

(a)

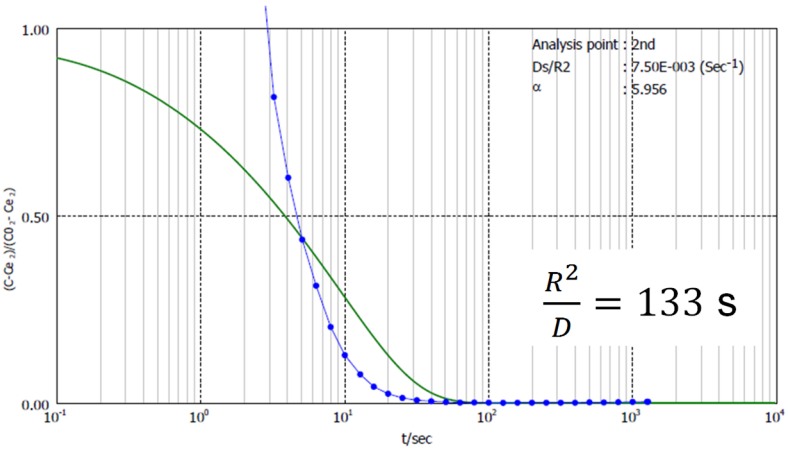

(b)

Figure 1. Experimental data obtained on a Belsorp Max and corresponding automated analysis using the adsorption rate analysis software Bel Dyna software tool. (a) Surface barrier model; (b) Diffusion model. The software assumes batch adsorption and linear equilibrium.

2. Theory

The traditional method to analyse the dynamics of a volumetric system is to convert the measured pressure into a fractional uptake. To understand the assumptions inherent in this approach it is useful to consider the schematic diagram of a volumetric system shown in Fig. 2.

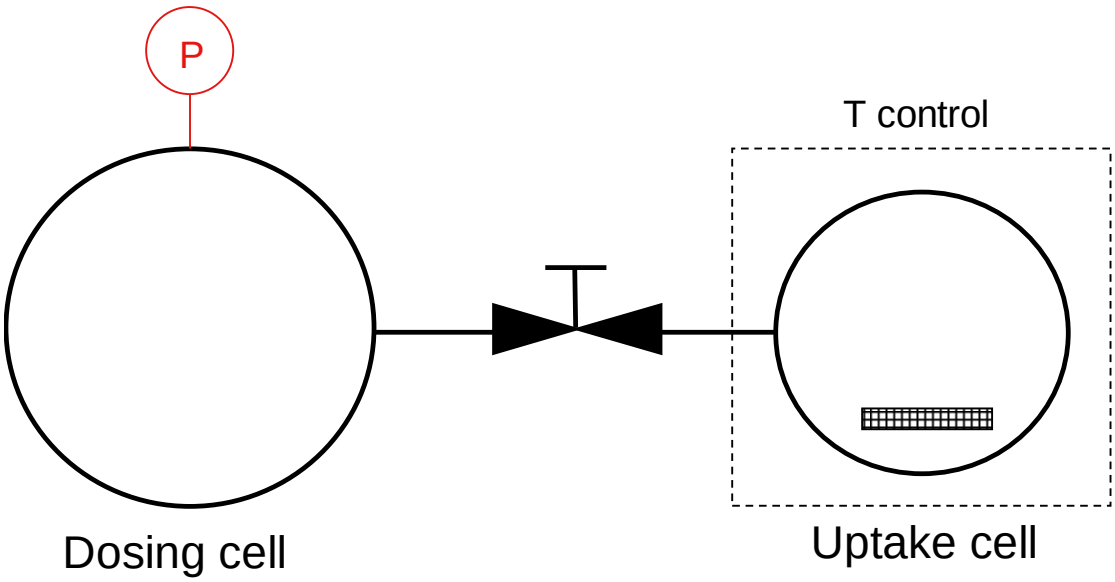

Figure 2. Schematic diagram of a volumetric system.

In commercial systems the pressure is measured on the dosing side, since the experiment is carried out by

1) starting from an equal pressure, P_{U0}, in the two cells
2) closing the valve that connects the two sides
3) increasing the pressure (in the case of an adsorption experiment) in the dosing side to P_{D0}
4) opening the valve and monitoring the pressure change to the final equilibrium point, P_{∞}

Knowing the temperature and the volumes of the two cells, from an equation of state (here the ideal gas state is assumed) it is possible to determine how many moles were present in the gas phase before opening the valve and at equilibrium, thus allowing by difference to determine the adsorbed amount at this step. Repeating the experiment additional points on the isotherm are obtained.

If the pressure as a function of time is recorded, in principle the dynamic response can be used to study mass transfer kinetics. The traditional approach is based on converting the measured pressure into a relative uptake assuming

$$\frac{q_t - q_0}{q_\infty - q_0} \approx \frac{P_D - P_0}{P_\infty - P_0} \quad (1)$$

where

$$P_0 = \frac{P_D^0 V_D + P_U^0 V_U}{V_D + V_U} \quad (2)$$

Equation 2 assumes that flow between the two cells is very fast compared to mass transfer, ie that the pressure equilibrates and *then* adsorption starts.

For diffusion in a sphere the solution to the diffusion equation assuming no resistance in the valve is given by Crank (1975)

$$\frac{q_t - q_0}{q_\infty - q_0} = 1 - \sum_{i=1}^{\infty} \frac{6\alpha(\alpha+1)}{9\alpha + 9 + \alpha^2\beta_i^2} \exp\left(-\beta_i^2 \frac{tD}{R^2}\right) \quad (3)$$

where:

$$\tan \beta_i = \frac{3\beta_i}{3 + \alpha\beta_i^2} \qquad \text{and} \qquad \alpha = \frac{3(V_D + V_U)}{4\pi R^3 K} \quad (4)$$

The assumption that the pressure between the two cells equilibrates instantaneously, ie that the valve and the lines between the dosing and uptake volumes do not contribute any resistance to the flow of gas, is clearly not physically realistic for short times and this explains why the experimental curves shown in Fig. 1 start above 1, since $P_D^0 > P_0$. The fact that for a fast system there is an uncertainty over the behaviour of the fractional uptake for short times does not allow to use the fractional uptake vs $\sqrt{t}$ plot (Ruthven, 1984) to distinguish between diffusion and surface barriers.

To include the effect of the valve, one has to use the analysis of the isothermal volumetric system presented by Brandani (1998). To aid the discussion the essential features of this model are presented below.

Assuming an ideal gas, the mass balance in the dosing volume can be written as

$$\frac{dn}{dt} = -\frac{V_D}{RT_D}\frac{dP_D}{dt} \quad (5)$$

and the mass balance in the uptake cell is given by

$$\frac{dn}{dt} = \frac{V_U}{RT_U}\frac{dP_U}{dt} + V_s\frac{d\bar{q}}{dt} \quad (6)$$

while the linearised flow through the valve can be written as

$$\frac{dn}{dt} = \bar{\chi}(P_D - P_U) \quad (7)$$

By combining Eqs 5-7 n can be eliminated and a set of two independent mass balances is obtained. Given that the combined uptake and dosing volumes are in a closed system the total number of moles does not change and is given by

$$N_{tot} = \frac{P_D^0 V_D}{RT_D} + \frac{P_U^0 V_U}{RT_U} + V_s\, q_0 = \frac{P_\infty V_D}{RT_D} + \frac{P_\infty V_U}{RT_U} + V_s\, q_\infty \quad (8)$$

The amount adsorbed at each step is then

$$V_s\,(q_\infty - q_0) = V_s \Delta q^* = \frac{(P_D^0 - P_\infty)V_D}{RT_D} - \frac{(P_\infty - P_U^0)V_U}{RT_U} \quad (9)$$

Brandani (1998) introduces the following dimensionless variables

$$Q = \frac{q - q_0}{q_\infty - q_0}; \quad \rho_D = \frac{P_D - P_U^0}{P_\infty - P_U^0}; \quad \rho_U = \frac{P_U - P_U^0}{P_\infty - P_U^0} \quad (10)$$

Two dimensionless groups are then obtained from the mass balances. These are 1/3 the ratios of the accumulation terms in the gas phase and the solid phase:

$$\gamma = \frac{1}{3RT_U}\frac{(P_\infty - P_U^0)V_U}{(q_\infty - q_0)V_S}; \quad \delta = \frac{1}{3RT_D}\frac{(P_\infty - P_U^0)V_D}{(q_\infty - q_0)V_S} \quad (11)$$

The expression for γ can also be modified to take into account that typically the uptake volume is represented as being formed by two regions at different temperatures: one is at room temperature and the submerged part is at the temperature of the solid phase. This corrects the accumulation of the gas phase of the uptake volume and requires the knowledge of the relative volumes of the uptake cell, which are typically measured from blank experiments using helium. Commercial systems will carry out this measurement automatically to improve the accuracy of the determination of the adsorption isotherm.

What should be clear is the fact that these two dimensionless groups cannot be set to arbitrary values, but are in fact calculated from the initial and final pressures in the system using Eq. 9.

If mass transfer in the solid follows the diffusion equation the problem is fully defined and can be solved in closed form assuming linear equilibrium

$$q^* - q_\infty = K_P(P_U - P_\infty) \quad (12)$$

Brandani (1998) shows that in this case

$$\frac{\rho_D}{\rho_D^0} = \frac{3\delta}{1+3\delta+3\gamma} + \sum_{i=1}^{\infty} a_i \exp\left(-\beta_i^2 \frac{D}{r^2} t\right) \quad (13)$$

where the eigenvalues of this system are obtained solving

$$\beta_i \cot \beta_i - z_i = 0 \quad (14)$$

and

$$z_i = 1 + \gamma\beta_i^2 + \frac{\omega\delta\beta_i^2}{\omega-\beta_i^2}\ ; \qquad a_i = \frac{2\omega^2\delta\beta_i^2}{2\omega^2\delta\beta_i^2+(\omega-\beta_i^2)^2(\beta_i^2+z_i^2-z_i+2\gamma\beta_i^2)} \qquad (15)$$

Note that there is an eigenvalue in each π interval plus an additional root in the interval where $\omega - \beta_i^2 = 0$ can occur.

This model contains a dimensionless parameter, ω, which is the ratio of the diffusion time constant and the time constant of the valve

$$\omega = \frac{RT_D}{V_D}\frac{\bar{\chi}r^2}{D} \qquad (16)$$

This means that a volumetric experiment run under linear conditions depends only on two parameters: ω and $\frac{r^2}{D}$.

For fast diffusing systems, Brandani (1998) explains clearly that the match of the fractional uptake at 50% should not be used to obtain the diffusional time constant. This is the method that the Bel Dyna software tool adopts.

While one can match the full model to the experimental data and obtain ω and $\frac{r^2}{D}$, it is useful to note that if the two time constants of the system are sufficiently different and diffusion is the slower process, it is possible to obtain the two constants from two different regions of the response. As pointed out by Brandani (1998) the initial response is dominated by the valve time constant, while the final approach to equilibrium is dominated by the diffusion time constant. To be able to identify clearly these two regions it is essential to plot a reduced pressure in a way that highlights the exponential decay in the long-time. This is achieved defining

$$\sigma_D = \frac{P_D - P_\infty}{P_D^0 - P_\infty} = \frac{\rho_D(P_\infty - P_U^0) + P_U^0 - P_\infty}{P_D^0 - P_\infty} \qquad (17)$$

Defined in this way the dimensionless pressure in the dosing cell (measured quantity) varies between 1 and 0. If this is plotted vs time on a semilog plot, it is possible to identify the short-time initial decay that allows to determine ω and the long-time asymptote (given by the first exponential in Eq. 13), which at this point will depend *only* on $\frac{r^2}{D}$.

Figure 3 shows the solution for the model equations for various values of the time constants. Figure 3a shows clearly that the long-time asymptotic slope is effectively independent of the valve time constant. Figure 3b shows clearly that the short-time asymptotic slope is independent of the diffusion time constant. Therefore the two time

constants can be determined *independently* from different regions of the dynamic response.

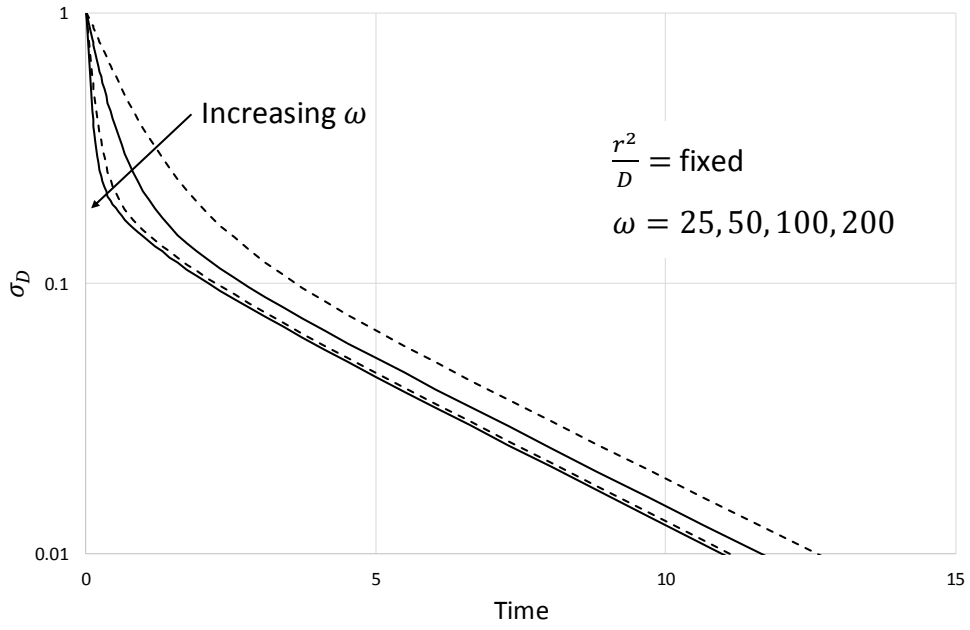

(3a)

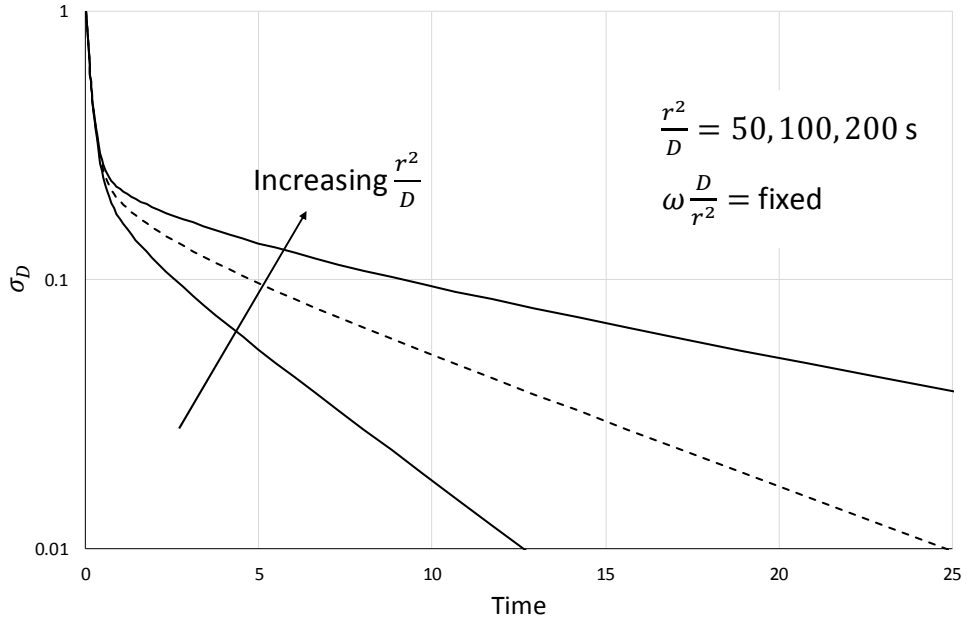

(3b)

Figure 3. Model dependence on two time constants: (a) effect of valve time constant; (b) effect of diffusion time constant. $\delta = 1$ and $\gamma = 0.5$, which are values representative of the system N_2 and LiLSX at −15 °C.

The same approach can also be used for the surface barrier or linear driving force (LDF) model. In this case the mass balance in the solid is

$$V_s \frac{d\bar{q}}{dt} = -A_s k(\bar{q} - q^*) \tag{18}$$

For spherical particles $A_s/V_s = 3/r$ and defining $\omega_{LDF} = \frac{\omega D}{kr}$ the following solution can be derived

$$\frac{\rho_{D,LDF}}{\rho_D^0} = \frac{3\delta}{1+3\delta+3\gamma} + \sum_{i=1}^{2} \frac{1}{s_i} \frac{(\delta\omega_{LDF}+\gamma s_i)(s_i+3)+s_i}{2\gamma s_i+3\gamma+1+\omega_{LDF}(\delta+\gamma)} \exp\left(s_i \frac{k}{r} t\right) \tag{19}$$

where

$$s_{1,2} = \frac{-[1+3\gamma+\omega_{LDF}(\delta+\gamma)] \pm \sqrt{[1+3\gamma+\omega_{LDF}(\delta+\gamma)]^2 - 4\gamma\omega_{LDF}(1+3\gamma+3\delta)}}{2\gamma} \tag{20}$$

The surface barrier model is the sum of two exponentials, so appears to be qualitatively similar to the diffusion model. Figure 4 shows that also in this case the initial response depends on the valve time constant while the asymptotic approach to equilibrium is determined by the mass transfer time constant.

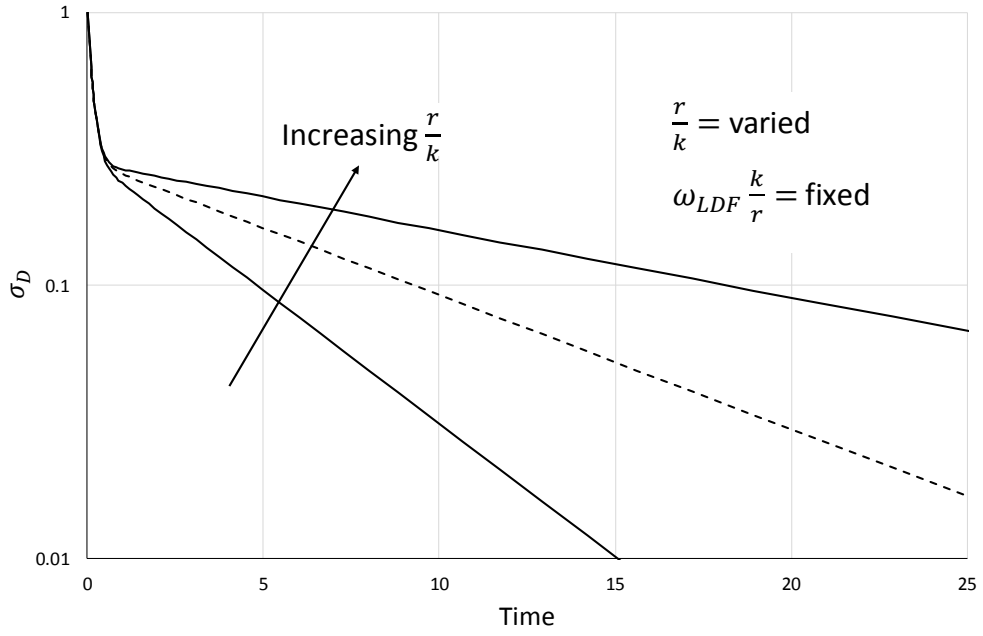

Figure 4. Surface barrier model dependence on two time constants ($\delta = 1$ and $\gamma = 0.5$)

If one compares the reduced pressure curves for the two models and realises that *only one adjustable parameter* determines the slope of the long-time asymptote, it is clear that the two models have significantly different intercepts of the long-time asymptote as can be seen from Fig. 5.

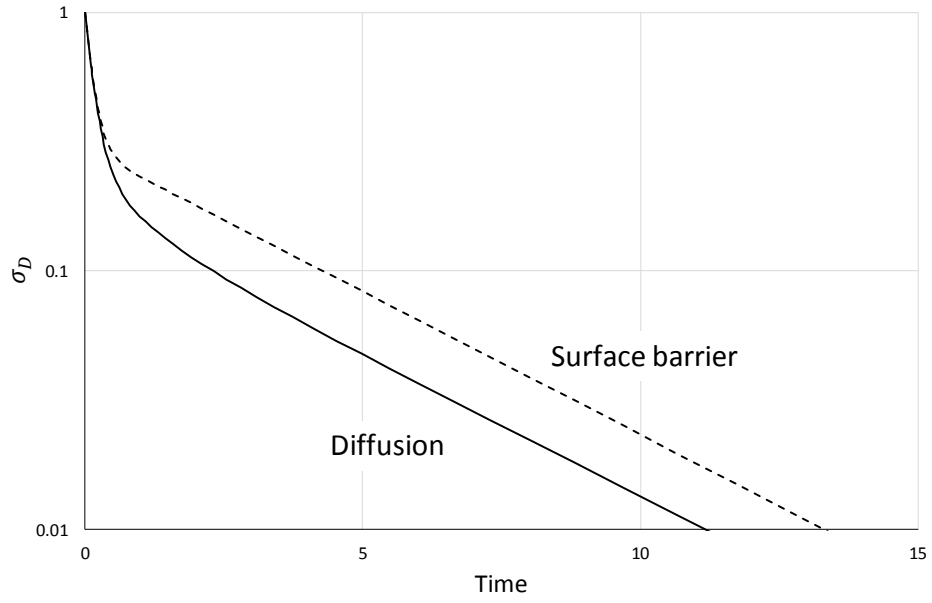

Figure 5. Comparison of surface barrier and diffusion models with the same long-time asymptotic rate.

Simply plotting the experimental data and the two models with the same long-time slope should allow to determine which model applies by inspection. Clearly intermediate intercepts can be obtained from a combined diffusion with surface barrier model.

3. Experimental

The LiLSX beads are commercial samples from Zeochem with a binder content between 10-18%. All experiments were performed with closely sized spherical beads with an average diameter of 1.27 mm. The diameter of each bead was measured with a Spi 15-997-0 digital caliper with a resolution of 0.01 mm and a corresponding accuracy of ±0.02 mm.

At Air Liquide the volumetric system used is a BELSORP-max. The number of samples that can be measured are 1-3 in the standard mode and 1-2 for the high accuracy mode (AFSMTM) with three sets of pressure transducers: 0 to 1 Torr (5 units); 0 to 10 Torr (2 units) and 0 to 1000 Torr (1 unit). In case of adsorption rate measurements only a single sample can be measured.

At the University of Edinburgh the volumetric system used for the kinetic experiments is a Quantachrome Autosorb-iQ2™. This system comprises two independent cells and dosing volumes (manifolds) with two sets of pressure transducers: 0 to 1 Torr; 0 to 10

Torr and 0 to 1000 Torr. The system allows the simultaneous testing of two samples in dynamic mode.

Prior to the experiments each sample was thermally regenerated at 390 °C under vacuum for 10 hours. The experiment consists in injecting a very small amount of N_2 in the uptake cell at constant temperature while the pressure is monitored. Once equilibrium is reached a new volume of N_2 is injected in the system and the process is repeated in small increments, which ensure linear conditions. Desorption experiments are carried out in a similar way, but in this case the pressure in the dosing volume is reduced opening the connection to the vacuum system for a short period of time. The pressure level is then automatically adjusted to a pre-set level with small additions of gas. These procedures are implemented by the control software of the two systems and no changes were made to these automated procedures.

Mercury porosimetry characterisation

Characterisation of the sample was carried out using a Quantachrome Poremaster® mercury porosimetry analyser. The system allows the characterisation of macro- and mesoporosity by means of repeated intrusions and extrusions of mercury from vacuum to high pressure. The experiment comprises low pressure and high pressure analyses. In the low pressure analysis, mercury is introduced in the sample cell (originally under vacuum) and pressurised using N_2 up to a pressure of 50 psi. At this pressure mercury will be able to fill the cell and the space between the particles. The first intrusion is followed by an extrusion and a repeat to check reproducibility. Once the low pressure analysis is complete, the sample cell is moved to the high pressure station, where the mercury contained inside the sample cell is now pushed inside the pores of the sample by gradually increasing the pressure up to 33000 psi using a piston. As for the low pressure analysis, intrusion is followed by an extrusion run and a repeat. To maximise accuracy, both analyses are carried out at the slowest rate of pressure increase.

The analysis requires the determination of the bulk volume of the sample. For this reason before starting the low pressure analysis, the weight of the sample cell, first empty and then completely filled with mercury, needs to be measured. Finally the weight of the cell right after the low pressure analysis (i.e. cell + sample + mercury) is measured. This information with the dry mass of the sample allows the software to determine the sample density.

4. Results and discussion

In order to be able to apply correctly the theory to the experiment one has to ensure that the underlying assumptions are valid. The key assumptions are:

1. The system is isothermal.
2. The system is linear.
3. There are no external or bed mass transfer resistances.

Both non-linearity and non-isothermal conditions will change the intercept of the long-time asymptote. Therefore experimental checks have to be used to make sure that assumptions 1 and 2 are valid.

To ensure isothermal conditions 1/16" stainless steel beads are added to the uptake cell to increase the thermal mass of the sample. This reduces significantly the adiabatic temperature rise and improves the heat transfer kinetics providing direct contact with the adsorbent beads and thus increasing the overall heat transfer surface. At the vacuum conditions of the experiment, the primary contribution to heat transfer is through radiative heat transfer. By performing the experiment with two different adsorbent sample masses it is possible to check if the system is isothermal, by ensuring that the mass transfer coefficient is the same for the two experiments. Experiments with different sample masses will also confirm if bed and external resistances are negligible.

To ensure linear conditions experiments with small pressure steps are performed and desorption experiments are carried out in the same pressure range. Under nonlinear conditions adsorption and desorption curves will differ (Ruthven, 1984).

In order to slow the adsorption process the temperature is lowered and larger beads in the batch are used. The main effect of reducing the temperature is to increase the equilibrium constant and therefore increase the effective diffusion time constant, $\frac{r^2}{D}$.

Figure 6 shows the two samples of different mass with the stainless steel beads.

Figure 6. 28 mg (left) and 46 mg (right) samples with 1792 mg of stainless steel beads.

Figure 7 shows the experimental curve at −15 °C for a pressure step close to 6 Torr. This pressure is chosen since it is in the middle range of the second pressure transducer and therefore gives a very good signal to noise ratio when converting the pressure of the dosing cell to the dimensionless pressure, Eq. 17. The data sampling rate is approximately 1 Hz and the data show clearly the long-time asymptotic behaviour. The mass transfer kinetics is very fast, as one would expect in a commercial sample designed for oxygen production and there is hardly any curvature at the short times. The long-time exponential decay is visible, therefore a reliable mass transfer time constant can be obtained, but simply looking at the data does not allow to determine which mass transfer mechanism prevails.

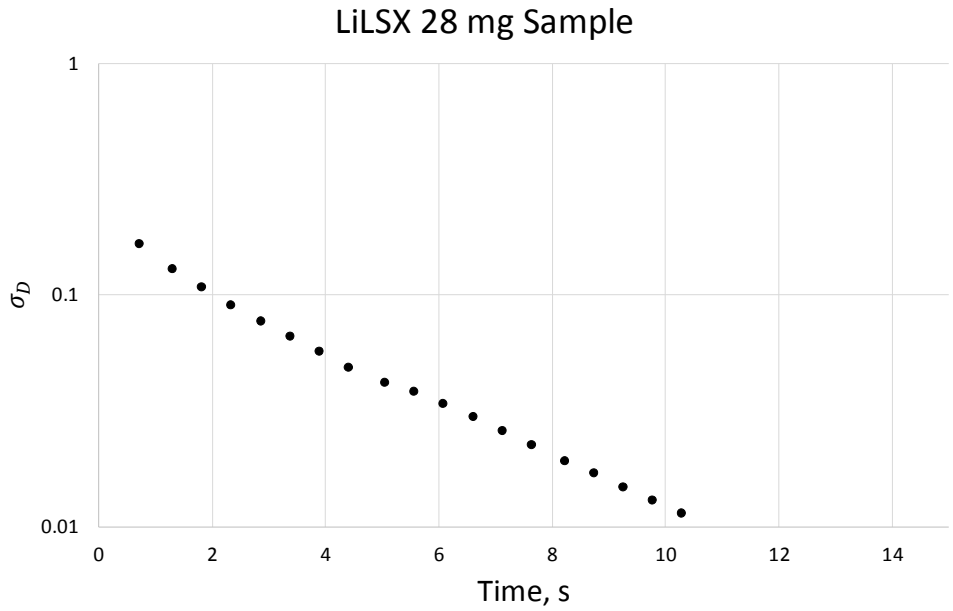

Figure 7. Experimental data plotted in semilog plot. P_U^0 = 4.85 Torr; P_D^0 = 7.12 Torr; P_∞ = 6.12 Torr.

Figure 8 shows the data and both the diffusion and surface barrier models that give the correct limiting slope. There is no doubt that the system behaves according to the diffusion model.

To make sure that the assumptions in the model are valid, Fig. 9 shows data for the 46 mg sample, along with the curve predicted using the diffusion time constant from the experiment with 28 mg. The intercepts are slightly different given that the sample mass is different and the gas lines in the two cells on the Autosorb-iQ2 are different, but the

excellent match demonstrates that the system is isothermal and that bed resistances are negligible.

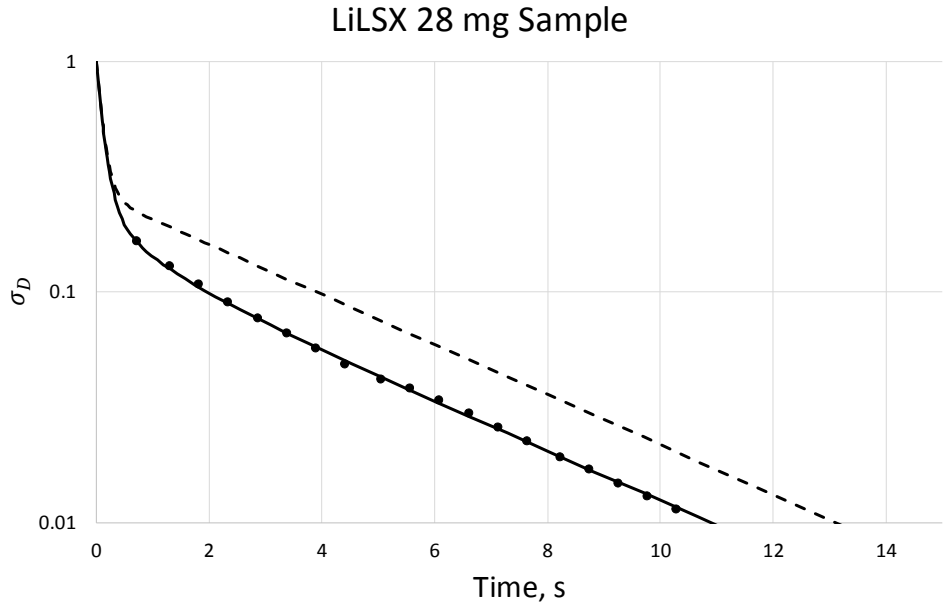

Figure 8. Experimental data with diffusion and surface barrier (dashed line) models that give the same long-time rate of decay.

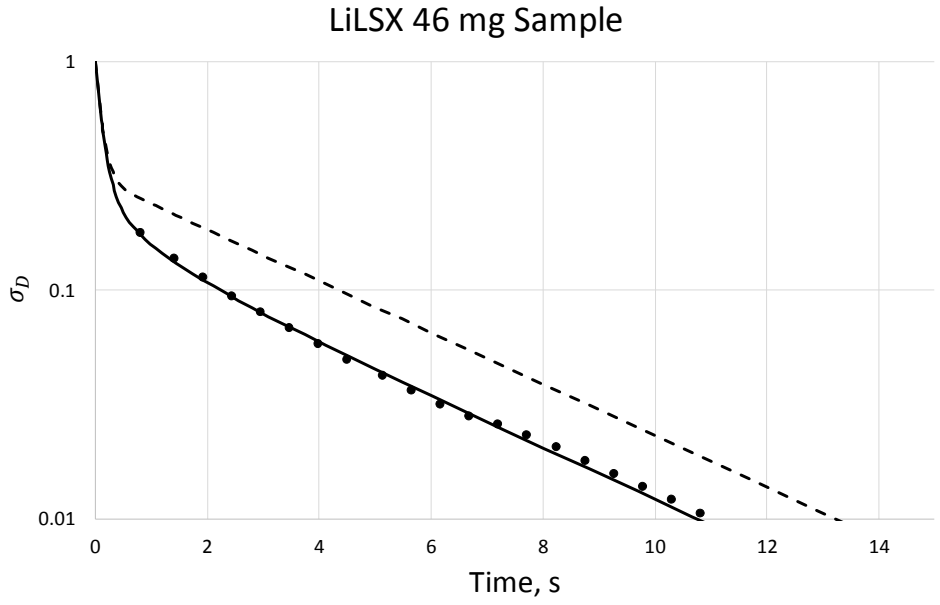

Figure 9. Experimental data with diffusion and surface barrier (dashed line) models. P_U^0 = 4.76 Torr; P_D^0 = 8.37 Torr; P_∞ = 6.16 Torr. Curves are calculated using the time constant fitted to the kinetic experiment on the 28 mg sample.

Figure 10 shows the adsorption and desorption data for the 46 mg sample. The overlap of the results confirms linearity, thus all model assumptions are valid.

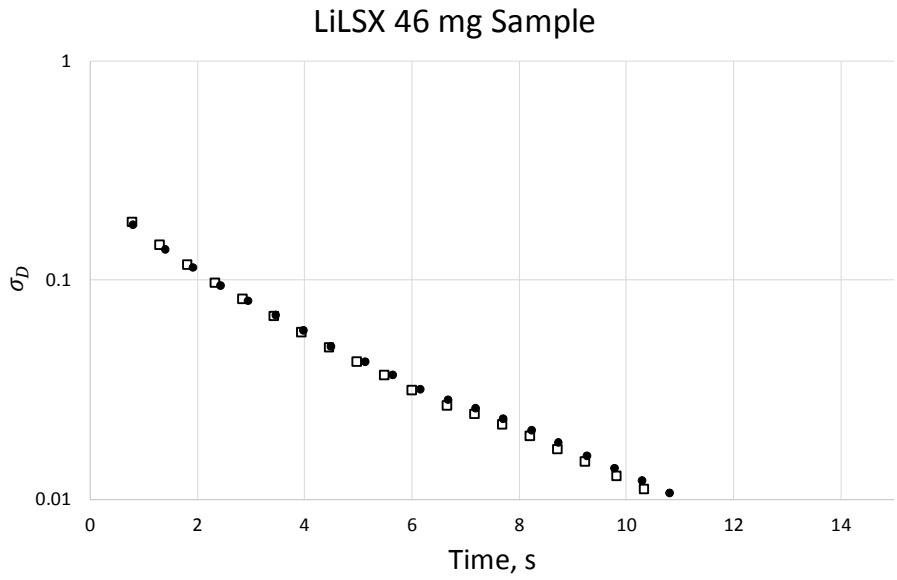

Figure 10. Data for adsorption (filled circle) and desorption (empty square) experiments at approximately 6 Torr.

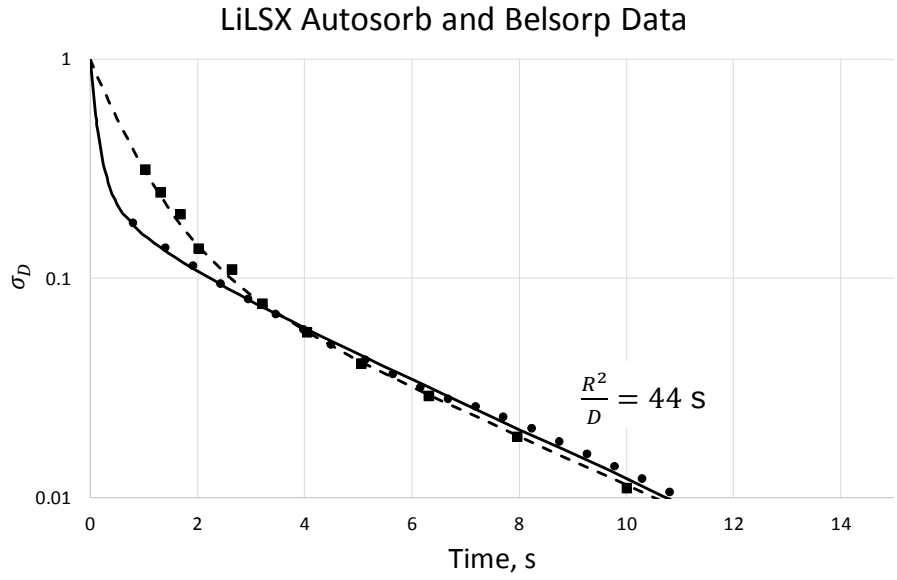

Figure 11. Comparison of kinetic experiments carried out on two commercial systems.

Figure 11 shows the results from the two instruments using the proposed semilog plot. Given that the volumes of commercial systems are similar it is possible to see that the long-time asymptotes on the two instruments have the same slope (ie the same diffusion

time constant) and very similar intercepts. Clearly the main difference in the two instruments lies in the connection between the dosing volume and the uptake cell. The valve resistance in the Belsorp system is much larger. This shows why the fractional uptake method seems to agree more with the surface barrier model, because this transfer limitation results in a simple exponential and will appear to be in agreement with the surface barrier model. It is therefore clear that comparing the fractional uptake curves predicted by the models will give the false impression that the system is controlled by a surface barrier as observed in Fig. 1. The other point that is quite important is that if this method is applied incorrectly and used to compare different materials, all the materials tested will appear to have very similar mass transfer coefficients.

On the other hand, if the proposed semilog plot of the dimensionless pressure is used, then the portion of the curve that contains most on the information on mass transfer kinetics becomes clearly visible and consistent results are obtained with both instruments. Comparison of different samples can then be carried out on the basis of the limiting slopes, for samples that have similar adsorption capacities.

Determination of the effective tortuosity

Figure 12 shows the pore size distribution obtained from the mercury porosimetry analysis. Clearly the sample shows a bimodal distribution of pores with a narrow peak at a pore diameter of 0.2 μm and a broader one at about 0.02 μm. Table 1 shows a summary of the relevant information obtained by the analysis. From the bulk volume of the sample measured in the low pressure analysis and the volume of intraparticle mercury intruded, the void fraction ε_p and the solid density ρ_p are calculated. Note that ρ_p represents the density of the solid including the micropores, as the mercury does not enter the micropores (Brandani et al., 2016).

Table 1. Summary of mercury porosimetry analysis

Mass	Bulk volume	Pore volume	ε_p	ρ_p	Mean pore diameter
1.014 g	1.0613 cm^3	0.3839 cm^3	0.362	1537 kg/m^3	0.1306 μm

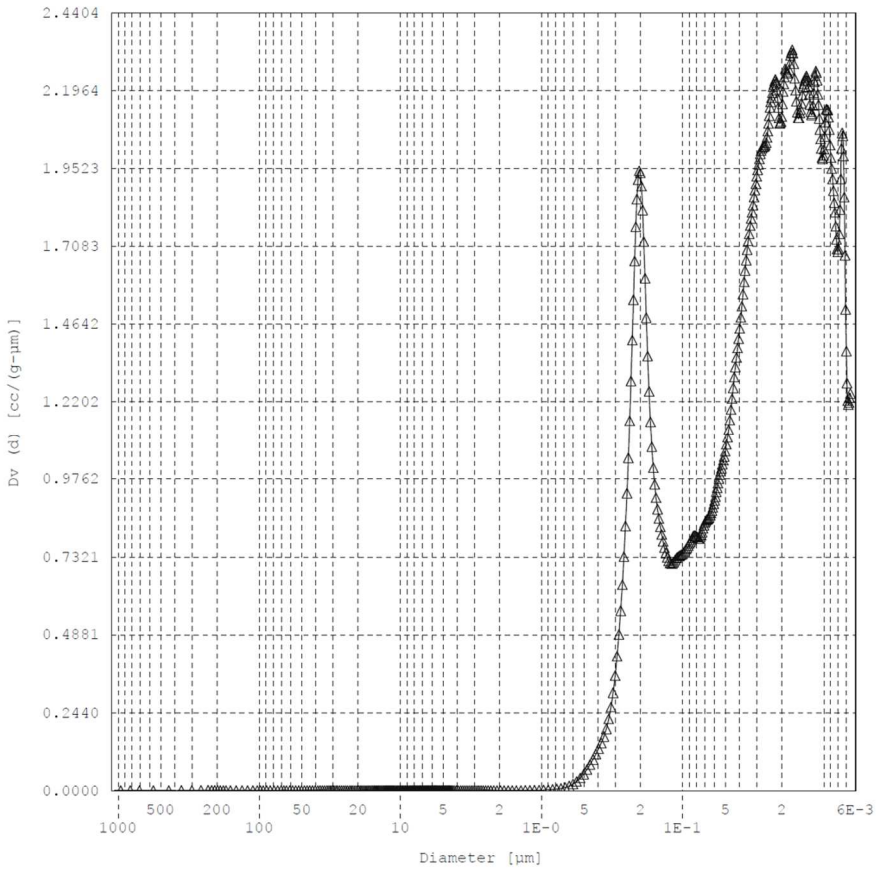

Figure 12: Pore size distribution of LiLSX sample from mercury porosimetry analysis

At the conditions of the volumetric experiment the transport of the pure gas molecules in the macropores is essentially dominated by Knudsen diffusion, D_K, with a very small contribution of viscous flow, D_{vis}. The two resistances operate in parallel so their contribution is generally assumed additive (Kärger et al. 2012) as defined in Eq. 21:

$$D_{macro} = D_K + D_{vis} \quad (21)$$

In which (Bird et al. 2000):

$$D_K = \frac{2}{3} r_p \sqrt{\frac{8RT}{\pi M}} \quad (22)$$

$$D_{vis} = \frac{P r_p^2}{8\eta} \quad (23)$$

where r is the pore radius, M is the molecular weight of the gas molecule and η is the viscosity. With regards to the Knudsen diffusivity, studies (Papadopoulos et al. 2007; Zalc et al. 2004) have suggested to use Derjaguin's correction (Levitz 1993):

$$D_{KD} = D_K \left[\frac{\langle r_p^2 \rangle}{2\langle r_p \rangle^2} - \frac{4}{13} \right] \approx \frac{9}{13} D_K \quad (24)$$

In a macropore process all contributions to the overall diffusion should be included in the expression of the effective macropore diffusivity, D_p^e, given by:

$$\frac{D_p^e}{r^2} = \frac{\varepsilon_p}{\tau\left[\varepsilon_p+(1-\varepsilon_p)\frac{dq^*}{dc}\right]}\frac{D_{macro}}{r^2} \quad (25)$$

Where τ is the pore tortuosity and $\frac{dq^*}{dc}$ is the derivative of the equilibrium isotherm. In volumetric experiments with small pressure steps

$$\frac{dq^*}{dc} \cong \frac{\Delta q^*}{\Delta c} \quad (26)$$

From Eq. 9 and the value of the solid density from Table 1 the value of Δq^* can be calculated, while Δc can be determined from the initial and final pressure in the sample cell.

D_p^e/r^2 is the quantity obtained from the kinetic analysis, it becomes clear that the effective pore tortuosity can be calculated by rearranging Eq. 25:

$$\tau = \frac{\varepsilon_p\, D_{macro}}{D_p^e\left[\varepsilon_p+(1-\varepsilon_p)\frac{\Delta q^*}{\Delta c}\right]} \quad (27)$$

The value of the tortuosity obtained is 3.13 which is in line with the typical ratio of ε_p/τ of about 0.1 (Kärger et al. 2012). Table 2 shows the values of the quantities used in Eq. 27.

Table 2. Summary of values used for the calculation of the pore tortuosity

Pellet radius, r	0.635 mm
Mean pore radius, r_p	0.065 μm
ε_p	0.362
D_{KD}	1.33×10^{-5} m^2/s
D_{vis}	2.9×10^{-8} m^2/s
D_p^e	9.2×10^{-9} m^2/s
$\frac{\Delta q^*}{\Delta c}$	263.8

Significance of diffusion time constant on process performance

In the production of oxygen using LiLSX beads, nitrogen is preferentially adsorbed due to equilibrium selectivity resulting from the interaction of the Li cations and the quadrupole moment in nitrogen. In a VSA process air is blown just above 1 bar during the adsorption step, where oxygen is produced with primarily argon as the main impurity. The adsorption bed is then regenerated using an evacuation step around 0.3-

0.5 bar, and enriched nitrogen is obtained. The desorption step is the one where mass transfer limitations will have a larger effect given that this system is macropore diffusion controlled. Industrial cycles are variants of the Skarstrom cycle (Ruthven et al. 1994). The performances of an industrial VSA oxygen unit may be characterized by its productivity expressed as the quantity of gas produced over the volume of adsorbent used ($Nm^3/h/m^3$) and by the specific energy consumption (kWh/Nm^3) for a given oxygen purity. The former having an impact on the capital costs of the unit (CAPEX) the latter being linked to the operating costs (OPEX). The factors that may affect these performances are the operating conditions, the hydrodynamic behaviour, the thermodynamic properties, the kinetics of adsorption which is important because VSA O_2 cycles are very short (Sun et al. 2005). To understand the impact of the different time constants – 44 s vs 133 s – obtained from the two methods of analysis, ie complete model vs fractional uptake with simplifying assumptions, we have considered the simulation of a typical VSA O_2 process. Using the same operating conditions and varying only the mass transfer constant for a given product purity we obtained that the process productivity drops by 14%, while the specific energy consumption increases by 15%.

5. Conclusions

The effective diffusivity of nitrogen on commercial LiLSX beads has been measured using two volumetric apparatuses. One of the two systems provided the option of running a traditional method of analysis of the kinetic experiments, but this was shown to yield the incorrect value of the time constant and suggested that the system was close to a surface barrier behaviour. These initial inconsistencies have been resolved through the use of a kinetic model that takes into account the effect of the valve and lines between the dosing and uptake volumes.

A new way of displaying the kinetic response of a volumetric system has been presented and applied to the commercial beads. For this system, the kinetic response can be divided into two regions which depend either on the valve time constant (short times) or the mass transfer time constant (long times), thus allowing a simple way of extracting the two time constants independently. The semilog plot of the dimensionless pressure of the dosing cell provides also a direct way to determine if the process is a diffusion process or is controlled by a surface barrier. In the case of nitrogen and LiLSX beads

the results are shown to be consistent with a pure diffusion process, as would be expected for this macropore diffusion controlled system.

The proposed method of analysing volumetric experiments to obtain kinetic information is predicated on the validity of the assumptions of the model used to extract the parameters. The experimental checks necessary to confirm the validity of the assumptions have been discussed in detail. Based on the results obtained we recommend that for the determination of kinetic constants in volumetric apparatuses, experiments should be carried out with different sample masses and with the addition of inert material that increases significantly the thermal mass of the sample. These experiments allow to confirm whether the system is isothermal. Small pressure steps have to be used to ensure linearity, which should also be confirmed by carrying out both adsorption and desorption experiments.

Avoiding the use of simplified methods of analysis, both laboratories obtained the same diffusion time constant for the samples. The comparison of the results on two systems highlighted the key difference in the gas flow characteristics between the dosing volume and the sample or uptake volume. The correct interpretation of the results provided also the explanation for the initial inconsistencies observed as a result of the use of the fractional uptake approach.

The practical importance of determining the correct diffusion time constant was evaluated by comparing the process performance using the correct value and that obtained from the simplified analysis. This comparison showed a difference of nearly 15% in both process productivity and specific energy consumption.

The beads were also characterised using mercury porosimetry. The pores size distribution and porosity information were combined with the volumetric experiments to derive the tortuosity of the beads, thus providing all the physical parameters needed to predict the effective diffusional time constant at the conditions of the separation process once the adsorption isotherm is known.

Dedication

This paper is dedicated to Professor Douglas Ruthven, with whom FB and SB have had the pleasure to collaborate over a period of more than 20 years. We hope that Doug Ruthven's influence on all of us, through his extensive body of work on kinetics of adsorption in nanoporous materials, has been evident in this contribution.

Notation

A_s	Surface of the solid, m^2
D_K	Knudsen diffusivity, $m^2\ s^{-1}$
D_{KD}	Knudsen diffusivity with Derjaguin's correction, $m^2\ s^{-1}$
D_{macro}	Macropore diffusivity, $m^2\ s^{-1}$
D_{vis}	Viscous diffusivity, $m^2\ s^{-1}$
D_p^e	Effective macropore diffusivity, $m^2\ s^{-1}$
k	Linear driving force constant, $m\ s^{-1}$
M	Molecular weight, $kg\ mol^{-1}$
P_D	Pressure in dosing volume, Pa
P_U	Pressure in uptake volume, Pa
q	Adsorbed amount, $mol\ m^{-3}$
q^*	Equilibrium concentration in adsorbed phase, $mol\ m^{-3}$
$\bar{q}$	Average concentration in adsorbed phase, $mol\ m^{-3}$
Q	Dimensionless adsorbed phase concentration
r	Particle radius, m
r_p	Average pore radius, m
R	Ideal gas constant, $J\ mol^{-1}\ K^{-1}$
t	Time, s
T_D	Temperature of dosing volume, K
T_U	Temperature of uptake volume, K
V_D	Dosing volume, m^3
V_S	Volume of the solid, m^3
V_U	Uptake volume, m^3

Greek symbols

β_i	Eigenvalues
δ	Dimensionless ratio of accumulation – dosing volume
ε_p	Macropore void fraction
γ	Dimensionless ratio of accumulation – uptake volume
ρ_D	Dimensionless pressure in dosing volume, Eq. 10
ρ_U	Dimensionless pressure in uptake volume, Eq. 10

σ_D	Dimensionless pressure in dosing volume, Eq. 17
τ	Effective tortuosity
$\bar{\chi}$	Valve constant mol s^{-1} Pa^{-1}
ω	Ratio of diffusion and valve time constants
ω_{LDF}	Ratio of surface barrier and valve time constants

References

Baerlocher Ch., McCusker L.B. and Olson D.H., Atlas of Zeolite Framework Types. 6th Ed. 2007, Elsevier, Amsterdam.

Bird, R. B., Stewart, W. E., Lightfoot, E. N., Transport Phenomena, 2nd Ed. 2002, New York, Wiley.

Brandani S., Analysis of the Piezometric Method for the Study of Diffusion in Microporous Solids: Isothermal Case. Adsorption, 1998. 4: 17–24.

Brandani S., Mangano E. and Sarkisov L. Net, Excess and Absolute Adsorption and Adsorption of Helium. Adsorption, 2016, 22: 261–276.

Crank J., The Mathematics of Diffusion. 2nd Ed. 1975, Oxford, Oxford University Press.

Hu X., Mangano E., Friedrich D. and Brandani S. Diffusion Mechanism of CO_2 in 13X Zeolite Beads. Adsorption, 2014. 20: 121–135.

Karger J. and Ruthven D.M., Diffusion in Zeolites and Other Microporous Solids. 1992, New York, Wiley.

Kärger J. and Ruthven D. M., Theodorou D. N., Diffusion in Nanoporous Materials. 2012, New York, Wiley-VCH.

Levitz, P., Knudsen Diffusion and Excitation Transfer in Random Porous Media. J. Phys. Chem. 1993. 97, 3813–3818

Papadopoulos, G. K., Theodorou, D. N., Vasenkov, S., Kärger, J., Mesoscopic Simulations of the Diffusivity of Ethane in Beds of NaX Zeolite Crystals: Comparison with Pulsed Field Gradient NMR Measurements. J. Chem. Phys. 2007. 126(094702), 1–8.

Ruthven D.M., Principles of Adsorption and Adsorption Processes. 1984, New York, Wiley.

Ruthven D.M., Farooq, S. and Knaebel K.S., Pressure Swing Adsorption. 1994, New York, Wiley.

Sun L.-M., Meunier F. and Baron G., Adsorption - Procédés et Applications. Techniques de l'Ingénieur. 2005. J2731 1–20.

Xu and Ruthven D.M., Diffusion of Oxygen and Nitrogen in 5A Zeolite Crystals and Commercial 5A Pellets. Chem. Eng. Sci. 1993. 48: 3307–3312.

Zalc, J. M., Reyes, S. C., Iglesia, E., The Effects of Diffusion Mechanism and Void Structure on Transport Rates and Tortuosity Factors in Complex Porous Structures. Chem. Eng. Sci. 2004. 59, 2947–2960.